

# Rotation Invariant Clustering of 3D Cell Nuclei Shapes\*

Patrick Wagner<sup>1</sup>, Jakob Paul Morath<sup>2</sup>, Arturo Zychlinsky<sup>2</sup>, Klaus-Robert Müller<sup>3,4,5</sup>, and Wojciech Samek<sup>1</sup>

**Abstract**—Cellular imaging with confocal fluorescence laser microscopy gave rise to many new insights into the cellular machinery. One interesting observation suggests that morphology of cell nucleus plays a key role for neutrophilic function, which is an essential part of the innate immune system of most mammals. Due to the increasing availability of high resolution 3D images coming from the microscope, machine learning becomes a promising tool for automatically discovering underlying hidden structures. Here, the major difficulty consists of selecting an appropriate representation for characterizing the morphology of cell nucleus. In this work we tackle this problem and propose a fully unsupervised mechanism for finding structure in high-throughput 3D image data. The key component of our approach is based on Generic Fourier Transform (GFT) for 2D images, which for 3D involves spherical coordinate transformation prior to fast Discrete Fourier Transformation. On top on GFT we apply dimensionality reduction with Principal Component Analysis, followed by generative cluster analysis with a Gaussian Mixture Model. We validate our new approach first on a synthetic 3D-MNIST dataset with random rotations, where quantitative and qualitative results confirm the applicability of the proposed pipeline for exploring shape space in a purely unsupervised manner. Then we apply our proposed technique to a new collected dataset of high resolution 3D images of neutrophilic nuclei suggesting a clustering model with six significant clusters of morphological cell nuclei prototypes. We visualize differences in the cell shape clusters by providing prototypical examples of neutrophilic cell nuclei.

## I. INTRODUCTION

Confocal laser fluorescence microscopy has become a standard tool allowing for observation of cellular components in remarkable three dimensional spatial resolution. With fluorescent proteins or dyes it is possible to make discrete cellular components visible in a highly specific manner. Analyzing these high-throughput microscopic data is crucial to understand cell biology. Moreover, establishing a data

driven pipeline can accelerate research by guiding experimental designs towards interesting questions concerning the relationship between environmental factors and morphological properties [1], [2]. This is a challenging task due to numerous computational considerations involved, ranging from image acquisition all the way to shape analysis and pattern recognition and interpretation.

Most previous studies characterizing cell nuclei focused on 2D microscopy, but since the cell lives in three dimensions, potentially important spatial information is neither observed nor considered [3]. Moreover, these studies focused mainly on differences in shapes between multiple experimental conditions yielding a supervised setting [3], [4], while fully unsupervised identification of morphological structures without any user annotations has only attracted little attention in cell biological applications [5]. However, since labels are often very expensive to acquire or are simply unknown, unsupervised data analysis is a promising approach for the discovery of structure in the data [1]. Most common methods for unsupervised learning include dimensionality reduction and clustering, where clustering can be used to extract subpopulations sharing similar properties according to some predefined metric [6]. The major difficulty of selecting an appropriate representation of 3D shapes is the need for invariance w.r.t. affine transformations. In particular, invariance w.r.t. rotations is the most important requirement for comparing shapes appropriately such that the same shape in different orientations yields the same representation.

Existing methods for 3D cell shape representation either use shape features like size or eccentricity [7], [8], which although rotation invariant, are too coarse for fine-grained discrimination [9], or solely rely on shape boundary information by extracting meshes from the voxel grid [3], [4]. The latter in the presence of noise yields unstable shape representations, thus affecting the reliability and introducing additional hyper-parameters highly specific to the data [9]. For a detailed review of shapes features in general we refer to [10] or [9]. Recently proposed methods for learning shape representation with data augmentation and Convolutional Neural Networks [11], [12] have been shown to be invariant only locally to small rotations but not globally to arbitrarily large transformations. In fact, it is an active field of research how to achieve the latter [13], [14].

We overcome the robustness and locality limitations by using generic Fourier transformation in the spherical image domain to obtain a reliable and rotation invariant shape feature representation of 3D cell nuclei images. Based on that we contribute a novel analysis pipeline that permits clustering of 3D images of neutrophil cell nuclei with respect

\*This work was supported by the German Ministry for Education and Research as Berlin Big Data Centre (01IS14013A) and Berlin Center for Machine Learning (01IS18037I). Partial funding by DFG is acknowledged (EXC 2046/1, project-ID: 390685689). This work was also supported by the Information & Communications Technology Planning & Evaluation (IITP) grant funded by the Korea government (No. 2017-0-00451). This publication only reflects the authors views. Funding agencies are not liable for any use that may be made of the information contained herein.

<sup>1</sup>P. Wagner (patrick.wagner@hhi.fraunhofer.de) and W. Samek (wojciech.samek@hhi.fraunhofer.de) are with Fraunhofer Heinrich Hertz Institute, 10587 Berlin, Germany.

<sup>2</sup>J. P. Morath (morath@mpiib-berlin.mpg.de) and A. Zychlinsky (zychlinsky@mpiib-berlin.mpg.de) are with Max Planck Institute for Infection Biology, 10117 Berlin, Germany.

<sup>3</sup>K.-R. Müller (klaus-robert.mueller@tu-berlin.de) is with the Technische Universität Berlin, 10587 Berlin, Germany.

<sup>4</sup>K.-R. Müller is with the Max Planck Institute for Informatics, 66123 Saarbrücken, Germany.

<sup>5</sup>K.-R. Müller is with the Korea University, Seoul 136-713, South Korea.

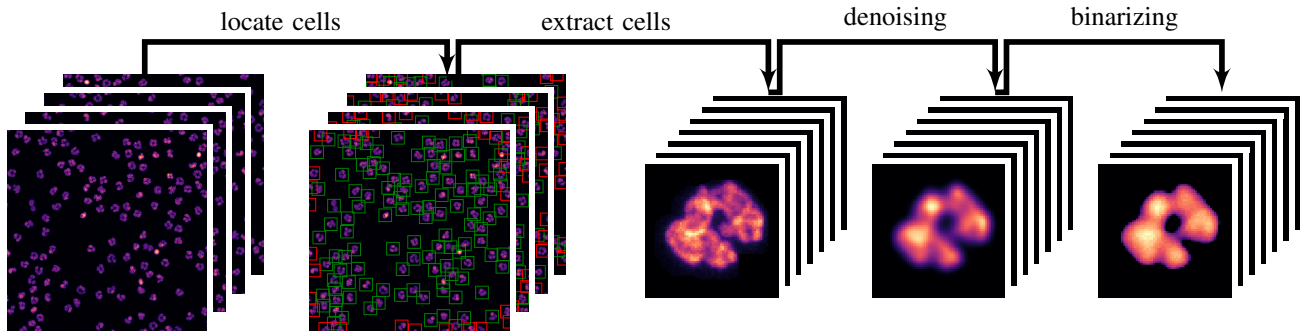


Fig. 1: Preprocessing of raw microscopy data as described in Section II-B, where each slice represents a 3D image as the summation along z-stack.

to their shapes. Members within one cluster share common morphological properties, thereby enabling the visualization and exploration of rotation invariant biological 3D images.

The rest of the paper is organized as follows. After giving an introduction to the biological background and the data in Section II, we describe our analysis pipeline in Section III. Quantitative evaluation of our method is performed on a synthetic 3D-MNIST dataset in Section IV-A. We apply our method to the neutrophil cell nuclei data in Section IV-B and conclude the paper with a discussion in Section V.

## II. BIOLOGICAL BACKGROUND & DATA

### A. Neutrophils

A commonly applied hypothesis states that structure determines the functional behaviour [15] [16] [17]. This also holds for neutrophils (also known as polymorphonuclear cells), which are the most abundant type white blood cells in humans. Patients with congenital neutrophil deficiencies suffer from severe infections that are often fatal [18], since they form an essential part of the innate immune system that migrate through tissue towards sites of infection. In 2004 [16], a new mechanism called *Neutrophil Extracellular Traps* (NETs) that enables neutrophils to kill bacteria by building extracellular traps consisting mostly of granular proteins was described. Neutrophils are characterized by their multi-lobed nuclei, typically exhibiting three or four lobes that are connected by thin DNA-containing filaments [15]. It is not known whether nuclear lobulation is required for NET formation. Neutrophils with hypolobulated nuclei (more than four) are associated with *Pelger-Huet anomaly*, which is caused by mutations in the gene encodings of the lamin B receptor [19]. Neutrophils with hypolobulated nuclei have deficiencies in various cellular functions like migrating through small openings. These observations strengthen the proposal that the morphology of the neutrophil's nucleus plays a role in neutrophilic cellular function [15], [16]. The analysis and categorization of neutrophil cell nuclei shapes obtained with confocal laser fluorescence microscopy offers the possibility of obtaining new insights into the morphological space.

### B. Data Aquisition & Preprocessing

In order to investigate cell nuclear morphologies, we gathered a blood sample from a random healthy subject and isolated neutrophils using density gradients similar to [20]. Then we stained the cells using *Draq5* as fluorescent DNA dye and used a *Leica TCS SP8* confocal microscope for cell imaging. Since raw data from the microscope comes as large scanned area with several dozen cells in it, preprocessing is an important step in the analysis pipeline (see Figure 1). In this paper we used thresholding, erosion and dilation techniques to automatically locate and extract individual cells [21]. This process returned 1525 samples in total, where in order to avoid artifacts we discarded samples that were too close to the image border. While raw data has spatial resolution of 90 nanometers per voxel yielding a  $128^3$  image grid per cell (about 115 micrometer cube which should be sufficient for unstimulated neutrophils), for the following experiments data was down-scaled to 180 nanometer per voxel yielding a  $64^3$  image grid followed by deconvolving each image with a microscope specific empirically measured point spread function using the iterative *Richardson-Lucy-Deconvolution* [22] [23] for three iterations. Since the marker protein *Draq5* does not stick homogeneously to the nucleus, images are binarized such that only shape features are taken into account. Since the shapes are more a flat disk than a round sphere, aligning the shape of interest to their principal components ensures that most variance is captured in the horizontal plane. This allows for convenient visualization by selecting the middle slice or summation along z-axis of the stack.

## III. ROTATION INVARIANT 3D SHAPE DESCRIPTOR AND ANALYSIS PIPELINE

This section introduces the main components of our analysis pipeline, namely the rotation invariant 3D shape descriptor (Section III-A), the dimensionality reduction method (Section III-B) and the clustering algorithm (Section III-C).

### A. Shape Feature Extraction

Fourier transformation is a well known and commonly used technique in signal processing for pattern analysis [24],

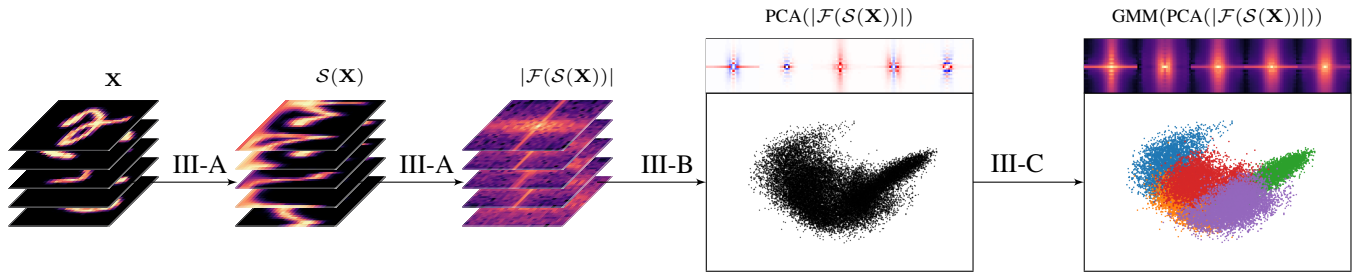


Fig. 2: Visualization of the proposed method as described in Section III for a randomly rotated subset of 3D-MNIST, where each slice represents a 3D image as the summation along z-stack.

where the output represents the image in the frequency domain, while the input image is the spatial domain equivalent. Acquiring shape features using Fourier directly are neither rotation invariant nor compact [9], [24]. Therefore [24] proposed a modified discrete polar Fourier transformation or *Generic Fourier Transform* (GFT) by first transforming the image in a regular two-dimensional rectangular polar image (similar to [25]). In this paper we extend this idea to 3D images by considering the spherical transformation.

Given a 3D image  $\mathbf{x}$  in Cartesian coordinates, the spherical transformation  $\mathcal{S}(\mathbf{x})$  with  $\mathcal{S} : \mathbb{R}^{X \times Y \times Z} \rightarrow \mathbb{R}^{\Gamma \times \Phi \times \Theta}$  is done by mapping regular spaced spherical coordinates to coordinates in Cartesian input image with radial resolution of  $\Gamma$  and polar and azimuthal resolution of  $\Phi$  and  $\Theta$ . This mapping is used to find the corresponding pixels in the input image. The value at spherical pixel coordinates are determined by linear spline interpolation of the corresponding Cartesian pixels. The resulting regular spherical grid can then be treated as regular image for a multidimensional discrete Fourier Transformation (DFT). In general the multidimensional DFT  $\mathcal{F}(\mathbf{x})$  converts an image into a same-sized complex-valued image in frequency domain. In case of DFT with 3D images in spherical coordinates  $\mathcal{F}(\mathcal{S}(\mathbf{x}))$ , the physical meanings of resulting coefficients are clear, i.e. the  $\gamma$ th radial frequency for  $0 \leq \gamma \leq \Gamma$  and  $\theta$ th polar and the  $\phi$ th azimuthal angular frequency respectively for  $0 \leq \theta \leq \Theta$  and  $0 \leq \phi \leq \Phi$ . The determination of the number of  $\gamma$ ,  $\phi$  and  $\theta$  for shape description is physically achievable, because shape features are usually captured by few lower frequencies. Furthermore, a rotation around the origin along each axis of a 3D image  $\mathbf{x}$  of  $\theta = (\theta_x, \theta_y, \theta_z)$  denoted as  $\mathcal{R}(\mathbf{x}, \theta)$ , translates into a shift in spherical coordinates. This is why in case of spherical representation rotational invariance naturally emerges due to the *shift theorem* of DFT by considering the magnitude of each complex coefficient, i.e.:

$$|\mathcal{F}(\mathcal{S}(\mathbf{x}))| = |\mathcal{F}(\mathcal{S}(\mathcal{R}(\mathbf{x}, \theta)))|$$

For the rest of this paper  $|\mathcal{F}(\mathcal{S}(\mathbf{x}))|$  is denoted as  $|\text{GFT}(\mathbf{x})|$  i.e. the Generic Fourier Transformation (GFT) of an 3D image.

### B. Dimensionality Reduction with PCA

Measuring similarities using Euclidean metric in high dimensional spaces is difficult due to the curse of dimen-

sionality and especially in the presence of noise. Reducing dimensionality prior to clustering is beneficial in order to avoid these limitations [6]. The most common technique is Principal Component Analysis (PCA), which aims to minimize squared residual loss while keeping as few dimensions as possible, and probably more important also results in denoised data [6]. In Figure 2 the first five leading eigenvectors are shown on top of the resulting 2D embedding. We used the (last large) eigengap criterion (difference between two successive eigenvalues) for selecting an appropriate number of principal components. In the case of data in frequency domain, whitening or sphering prior to fitting a cluster model yield much better and more robust results, since this scaling ensures zero mean and co-variance equal to the identity. Since we used scatter criteria to select a clustering model, whitening also enhances applicability of within and between scatter criteria for clusters.

### C. Clustering with Gaussian Mixture Model

Recall our motivation that searching for models with discrete latent variables (i.e., clusters) might help to identify morphological prototypes. Since the transition from one to another type of nucleus, if any, does not happen instantaneously, a probabilistic Gaussian Mixture model (GMM) seems to be a natural choice. In general a GMM is a linear superposition of Gaussian components, providing a rich classes of density models commonly optimized with the expectation maximization algorithm [6]. Furthermore we constraint the co-variance of each component such that all off diagonal elements are zero. This constraint in combination with whitened features yielded robust results when scatter criteria was used for model selection. In many practical applications the number of clusters is not known in advance. A commonly used technique leads to several maximum likelihood estimates for a ranging number of clusters, where the optimal number of cluster is chosen according to multiple available criteria. Although model likelihood of training data increases with increasing number of clusters, the likelihood for test data should saturate. A selection criterion, which was used in this paper and is known to perform well when the local densities are spherical, is the *Calinski-Harabasz-Index* [26].

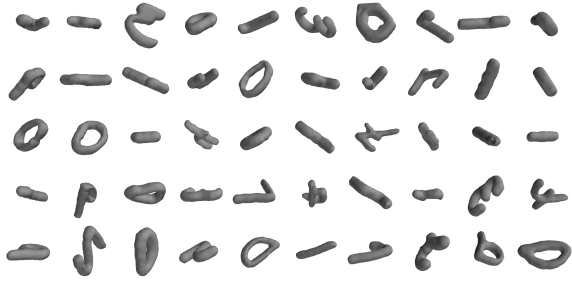


Fig. 3: Random examples from the synthetic 3D-MNIST where each sample is rotated randomly.

TABLE I: Results of experiment described in Section IV-A.

	full	PCA	Whiten PCA
Original 3D-MNIST			
raw	$0.72 \pm 0.23$	<b><math>0.90 \pm 0.16</math></b>	$0.82 \pm 0.29$
ART	$0.59 \pm 0.08$	$0.89 \pm 0.02$	$0.89 \pm 0.02$
GFT	$0.57 \pm 0.13$	$0.84 \pm 0.08$	$0.79 \pm 0.13$
ART	$0.27 \pm 0.04$	$0.72 \pm 0.09$	$0.79 \pm 0.04$
GFT	$0.38 \pm 0.15$	$0.81 \pm 0.06$	<b><math>0.90 \pm 0.06</math></b>
$\overline{\text{ART}}$	$0.35 \pm 0.14$	$0.68 \pm 0.16$	$0.74 \pm 0.16$
$\overline{\text{GFT}}$	$0.62 \pm 0.11$	$0.80 \pm 0.03$	$0.84 \pm 0.10$
Rotated 3D-MNIST			
raw	$0.37 \pm 0.10$	$0.45 \pm 0.12$	$0.52 \pm 0.11$
ART	$0.43 \pm 0.08$	$0.60 \pm 0.08$	$0.47 \pm 0.16$
GFT	$0.30 \pm 0.10$	$0.54 \pm 0.02$	$0.54 \pm 0.03$
ART	$0.27 \pm 0.07$	$0.71 \pm 0.09$	$0.79 \pm 0.04$
GFT	$0.34 \pm 0.16$	$0.81 \pm 0.05$	<b><math>0.90 \pm 0.07</math></b>
$\overline{\text{ART}}$	$0.37 \pm 0.18$	$0.72 \pm 0.16$	$0.77 \pm 0.12$
$\overline{\text{GFT}}$	$0.66 \pm 0.08$	$0.81 \pm 0.03$	$0.86 \pm 0.10$

#### IV. EXPERIMENTS & RESULTS

Before applying the proposed method to the unlabelled nuclei data, we evaluate its performance on a labelled dataset. For that we create a synthetic 3D-MNIST dataset by expanding pixel values of original MNIST<sup>1</sup> in positive and negative z-direction with a decay such that the resulting shape is something between a flat disk and a sphere (which is also the case for neutrophil cell nuclei). Figure 3 shows some examples of this dataset.

##### A. Evaluation on synthetic 3D-MNIST

To highlight and evaluate the key component of our proposed approach, we conducted the following experiment, where each pair of features and dimensionality reduction technique is applied to both original dataset (Original 3D-MNIST) and the same dataset consisting of random rotations (Rotated 3D-MNIST) prior to applying GMM. GMM was the same for all pipelines (five components with best likelihood fit out of 20 initializations). Each experiment is conducted on a subset of synthetic 3D-MNIST consisting of five classes (0,1,2,3,4). In order to compensate for small but high dimensional data, a repeated random subsampling validation with 30 splits is performed such that training data consisted of thousand samples in each split.

<sup>1</sup><http://yann.lecun.com/exdb/mnist/>

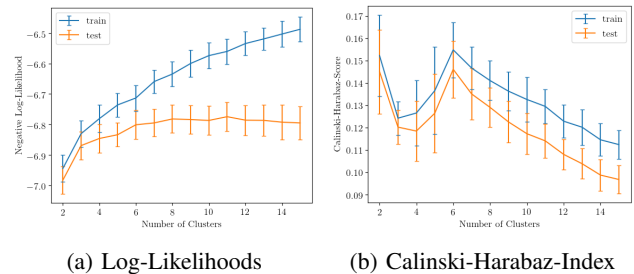


Fig. 4: Results of number of clusters analysis as described in Section IV-B.

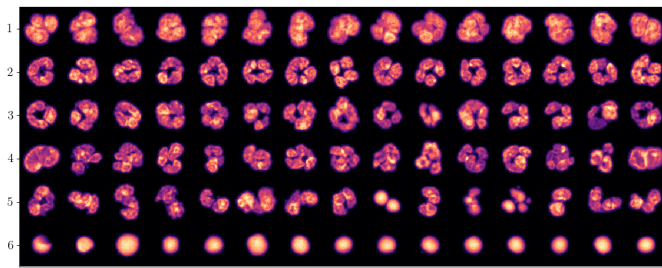
Besides our proposed shape feature |GFT|, we also considered the Angular Radial Transformation (ART) [27] feature, which is a region-based image descriptor in MPEG-7 [28], of order  $M_\theta=M_\phi=N=6$  as baseline. As an additional baseline we considered the raw image domain features without any further preprocessing, which is denoted as *raw* in the left column of Table I. In addition to rotational invariance due to the magnitude of both GFT and ART, we also evaluated the performance of normalized magnitudes for scale invariance, denoted as  $\overline{\text{GFT}}$  and  $\overline{\text{ART}}$  and also raw complex features GFT and ART where real and imaginary parts are concatenated. To demonstrate the importance of dimensionality reduction, each experiment is applied with three scenarios. As a baseline the first pipeline applies GMM directly on the input features without any dimensionality reduction in between (denoted as *full* in the upper row of Table I). The second and third applies PCA with 6 leading components, where in addition the third applies whitening PCA prior to applying GMM.

Table I shows the results of this experiment reported as accuracies with respective standard deviations, where the assignment between ground truth label and cluster assignment is solved with the *Kuhn-Munkres algorithm* [29]. In the case of the original MNIST all methods yield considerable results, except for GMM in frequency domain without dimensionality reduction. Note that invariance to scaling by normalizing is not beneficial for clustering 3D-MNIST. In case of rotated 3D-MNIST only using the magnitude of proposed shape features give considerable results, where whitening PCA for |GFT| on rotated 3D-MNIST yield best results, similar to PCA on raw original 3D-MNIST.

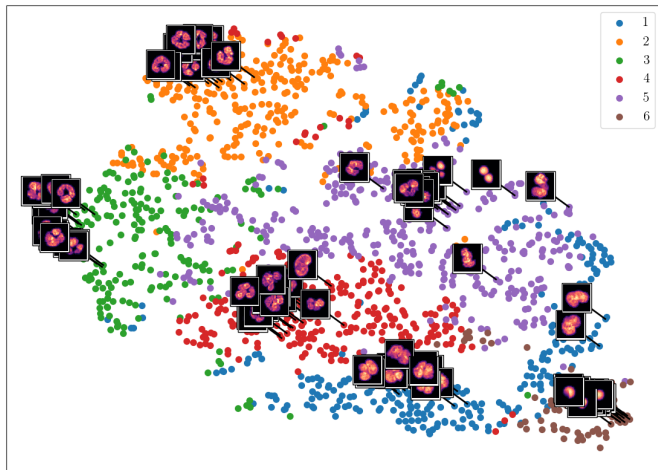
These results demonstrate that the proposed method is capable of obtaining meaningful embeddings and cluster models with respect to the 3D shapes invariant to the rotation.

##### B. Experiment with 3D neutrophil cell nuclei

Recall our collected dataset from Section II-B consisting of 1525 preprocessed samples. Again, the magnitudes of proposed GFT features are extracted prior to whitening with PCA, where the number of components was set to 6 components. Cluster analysis is conducted as described in Section III-C for  $k = 2, \dots, 16$ , where again we applied random subsampling cross-validation with 30 splits with equal train and test size to investigate likelihoods on unseen data.



(a) 15 most likely samples for each of the six clusters.



(b) TSNE-Embedding.

Fig. 5: Analysis of the neutrophil cell nuclei dataset with the proposed method.

Please note how the test likelihood in Figure 4a saturates after six clusters, which also coincides with the sharp peak of Calinski-Harabaz-Index at six clusters in Figure 4b. The vertical lines in each plot indicating the standard deviation for each number of clusters cross-validation respectively. This observation suggests that there are six clusters of shapes, which is of main interest for biological application, since it reveals the hidden structure of shape space of neutrophil cell nuclei. The feature embedding and clustering model can be used to facilitate interpretation by delivering convincing visualizations.

Figure 5a shows the 15 most likely (prototypical) samples for each of the six clusters as the summation along the z-stack. One can observe how the corresponding shapes in fact are similar within and dissimilar across clusters. E.g. cluster 6 contains quite dense nuclei which are probably not neutrophils but rather lymphocytes or monocytes, cluster 5 contains two-lobbed nuclei which could also be eosinophils. Cluster 2, 3 and 4 contain nuclei with a emphasized lobulation. These observations can facilitate further studies, which e.g. may determine whether the different members of each cluster have different cellular functions. For better visualization Figure 5b shows two dimensional *t-Distributed Stochastic Neighbor Embedding* (t-SNE) [30] of the proposed shapes features, where the clusters and samples of Figure 5a are color-coded and plotted onto the embedding.

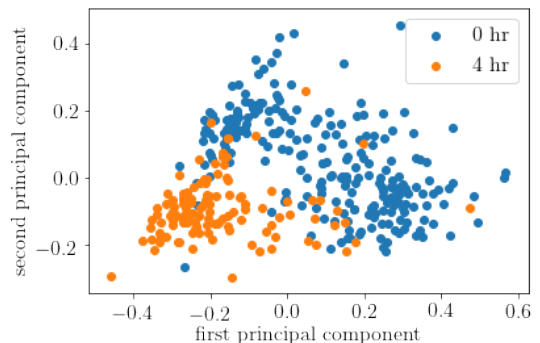


Fig. 6: PCA embedding showing effect of violation of i.i.d. assumption as described in section IV-B.

To further investigate the dependencies between method of data acquisition and the resulting cell nuclei shape space, we collected a dataset from the same blood sample, but one part imaged directly and the other part four hours after acquisition. In Figure 6 the resulting embedding on the first two principal components is shown, where one can easily observe a systematic shift to the lower left corner as the time between acquisition and imaging increases, i.e. the nuclei shapes become more dense or clumpy. The proposed rotation invariant representation for the first time enables the biological expert to perform this type of analyses.

## V. CONCLUSION

In this paper we proposed a novel rotation-invariant clustering method for 3D data based on GFT features, PCA-based dimensionality reduction and the GMM algorithm. Quantitative evaluation on a synthetic 3D-MNIST dataset demonstrated the applicability of this method. Based on the results on 3D neutrophil cell nuclei data, we can conclude that there are distinct morphological conformations justifying a clustering model with six clusters. Furthermore, our method enables further similar investigations with regard to the nuclear morphology of certain cell types, e.g. images of serum starved and proliferating fibroblast cells [3].

In future work we will apply explanation methods [31], [32] to better understand the specific features of each cluster. Furthermore we will consider more powerful techniques for dimensionality reduction such as Kernel PCA [33], Spectral Embedding [34], or Stationary Subspace Analysis [35].

## VI. AUTHOR CONTRIBUTION

PW and WS contributed to theory and methods. PW, WS and KRM designed the experiments, performed the analysis and wrote the paper. AZ helped posing the biological question and JPM participated in posing the biological question and generated the raw data.

## REFERENCES

- [1] A. C. Dufour, T.-Y. Liu, C. Ducroz, R. Tournemene, B. Cummings, R. Thibeaux, N. Guillen, A. O. Hero, and J.-C. Olivo-Marin, "Signal processing challenges in quantitative 3-d cell morphology: More than meets the eye," *IEEE Signal Process. Mag.*, vol. 32, no. 1, pp. 30–40, 2015.

- [2] K. Xu, V. G. Kim, Q. Huang, N. Mitra, and E. Kalogerakis, "Data-driven shape analysis and processing," in *SIGGRAPH ASIA 2016 Courses*, 2016, p. 4.
- [3] A. A. Kalinin, A. Allyn-Feuer, A. Ade, G.-V. Fon, W. Meixner, D. Dilworth, R. Jeffrey, G. A. Higgins, G. Zheng, A. Creekmore *et al.*, "3d cell nuclear morphology: microscopy imaging dataset and voxel-based morphometry classification results," *bioRxiv:208207*, 2017.
- [4] C. Ducroz, J.-C. Olivo-Marin, and A. Dufour, "Characterization of cell shape and deformation in 3d using spherical harmonics," in *IEEE Int. Symp. Biomed. Imaging*, 2012, pp. 848–851.
- [5] C. Sommer and D. W. Gerlich, "Machine learning in cell biology—teaching computers to recognize phenotypes," *J Cell Sci*, pp. jcs-123 604, 2013.
- [6] C. M. Bishop, *Pattern Recognition and Machine Learning*. Springer, 2006.
- [7] Q. Zhong, A. G. Busetto, J. P. Fededa, J. M. Buhmann, and D. W. Gerlich, "Unsupervised modeling of cell morphology dynamics for time-lapse microscopy," *nature methods*, vol. 9, no. 7, p. 711, 2012.
- [8] M. Webster, K. L. Witkin, and O. Cohen-Fix, "Sizing up the nucleus: nuclear shape, size and nuclear-envelope assembly," *J. Cell Sci.*, vol. 122, no. 10, pp. 1477–1486, 2009.
- [9] D. Zhang and G. Lu, "Review of shape representation and description techniques," *Pattern Recognit.*, vol. 37, no. 1, pp. 1–19, 2004.
- [10] I. L. Dryden and K. V. Mardia, *Statistical Shape Analysis: With Applications in R*. John Wiley & Sons, 2016.
- [11] Y. LeCun, Y. Bengio, and G. Hinton, "Deep learning," *Nature*, vol. 521, no. 7553, p. 436, 2015.
- [12] G. E. Hinton, A. Krizhevsky, and S. D. Wang, "Transforming auto-encoders," in *Int. Conf. Artif. Neural Netw.*, 2011, pp. 44–51.
- [13] X. Zhang, L. Liu, Y. Xie, J. Chen, L. Wu, and M. Pietikainen, "Rotation invariant local binary convolution neural networks," in *Proceedings of the IEEE International Conference on Computer Vision*, 2017, pp. 1210–1219.
- [14] A. Bietti and J. Mairal, "Invariance and stability of deep convolutional representations," in *Advances in Neural Information Processing Systems*, 2017, pp. 6210–6220.
- [15] L. O. Carvalho, E. N. Aquino, A. C. D. Neves, and W. Fontes, "The neutrophil nucleus and its role in neutrophilic function," *J. Cell Biochem.*, vol. 116, no. 9, pp. 1831–1836, 2015.
- [16] V. Brinkmann, U. Reichard, C. Goosmann, B. Fauler, Y. Uhlemann, D. S. Weiss, Y. Weinrauch, and A. Zychlinsky, "Neutrophil extracellular traps kill bacteria," *Science*, vol. 303, no. 5663, pp. 1532–1535, 2004.
- [17] W. Zhao, D. K. Fogg, and M. J. Kaplan, "A novel image-based quantitative method for the characterization of netosis," *J. Immunol. Meth.*, vol. 423, pp. 104–110, 2015.
- [18] B. Amulic, C. Cazalet, G. L. Hayes, K. D. Metzler, and A. Zychlinsky, "Neutrophil function: from mechanisms to disease," *Ann. Rev. Immunol.*, vol. 30, pp. 459–489, 2012.
- [19] K. Hoffmann, C. K. Dreger, A. L. Olins, D. E. Olins, L. D. Shultz, B. Lucke, H. Karl, R. Kaps, D. Müller, A. Vayá *et al.*, "Mutations in the gene encoding the lamin b receptor produce an altered nuclear morphology in granulocytes (pelger-huet anomaly)," *Nature Genet.*, vol. 31, no. 4, p. 410, 2002.
- [20] D. B. Kuhns, D. A. L. Priel, J. Chu, and K. A. Zarembek, "Isolation and functional analysis of human neutrophils," *Current protocols in immunology*, vol. 111, no. 1, pp. 7–23, 2015.
- [21] R. Ahasan, A. U. Ratul, and A. Bakibillah, "White blood cells nucleus segmentation from microscopic images of strained peripheral blood film during leukemia and normal condition," in *Int. Conf. Inform. Elect. Vis.*, 2016, pp. 361–366.
- [22] W. H. Richardson, "Bayesian-based iterative method of image restoration," *J. Opt. Soc. Am.*, vol. 62, no. 1, pp. 55–59, 1972.
- [23] L. B. Lucy, "An iterative technique for the rectification of observed distributions," *Astron. J.*, vol. 79, p. 745, 1974.
- [24] D. Zhang and G. Lu, "Generic fourier descriptor for shape-based image retrieval," in *IEEE Int. Conf. Multimedia Expo*, vol. 1, 2002, pp. 425–428.
- [25] Q. Wang, O. Ronneberger, and H. Burkhardt, "Fourier analysis in polar and spherical coordinates," *Albert-Ludwigs-Universität Freiburg*, 2008.
- [26] T. Caliński and J. Harabasz, "A dendrite method for cluster analysis," *Commun. Stat. Theory Meth.*, vol. 3, no. 1, pp. 1–27, 1974.
- [27] J. Ricard, D. Coeurjolly, and A. Baskurt, "Generalizations of angular radial transform for 2d and 3d shape retrieval," *Pattern Recogn. Lett.*, vol. 26, no. 14, pp. 2174–2186, 2005.
- [28] M. Bober, "Mpeg-7 visual shape descriptors," *IEEE Trans. Circuits Syst. Video Technol.*, vol. 11, no. 6, pp. 716–719, 2001.
- [29] J. Munkres, "Algorithms for the assignment and transportation problems," *J. Soc. Ind. Appl. Math.*, vol. 5, no. 1, pp. 32–38, 1957.
- [30] L. Van Der Maaten, E. Postma, and J. Van den Herik, "Dimensionality reduction: A comparative review," *J. Mach. Learn. Res.*, vol. 10, pp. 66–71, 2009.
- [31] W. Samek, T. Wiegand, and K.-R. Müller, "Explainable artificial intelligence: Understanding, visualizing and interpreting deep learning models," *ITU Journal: ICT Discoveries - Special Issue 1 - The Impact of Artificial Intelligence (AI) on Communication Networks and Services*, vol. 1, no. 1, pp. 39–48, 2018.
- [32] S. Lopuschkin, S. Wäldchen, A. Binder, G. Montavon, W. Samek, and K.-R. Müller, "Unmasking clever hans predictors and assessing what machines really learn," *Nature Communications*, vol. 10, p. 1096, 2019.
- [33] S. Mika, B. Schölkopf, A. J. Smola, K.-R. Müller, M. Scholz, and G. Rätsch, "Kernel pca and de-noising in feature spaces," in *Adv. Neural Inf. Process. Syst.*, 1999, pp. 536–542.
- [34] A. Y. Ng, M. I. Jordan, and Y. Weiss, "On spectral clustering: Analysis and an algorithm," in *Adv. Neural Inf. Process. Syst.*, 2002, pp. 849–856.
- [35] S. Kaltenstadler, S. Nakajima, K.-R. Müller, and W. Samek, "Wasserstein stationary subspace analysis," *IEEE Journal of Selected Topics in Signal Processing*, vol. 12, no. 6, pp. 1213–1223, 2018.